Prediction of Cellular Structure in Free Expansion of Viscoelastic Media

KISHORE JOSHI,* JAMES G. LEE,† MUHAMMAD A. SHAFI,‡ RAYMOND W. FLUMERFELT§

Department of Chemical Engineering, Texas A&M University, College Station, Texas 77843

Received 29 December 1996; accepted 24 January 1997

ABSTRACT: A systematic model is presented for a free expansion polymer foaming process that includes simultaneous nucleation and bubble growth. An influence volume approach, which couples nucleation and bubble growth, is used to account for the limited supply of dissolved gas. The melt rheology is described using the Larson viscoelastic model. The initial conditions are obtained at the upper bound of critical cluster size under conditions of elastic deformation. The resulting set of equations are solved using a combination of numerical techniques. A parametric study is conducted to examine the effects of key process variables on bubble growth, nucleation, and final bubble size distribution. It shows that the factors influencing nucleation and growth affect the ultimate bubble sizes and their distribution. The Gibbs number, a dimensionless measure of the barrier to overcome for nucleation, has the strongest impact on the cellular structure of the foam. © 1998 John Wiley & Sons, Inc. J Appl Polym Sci **67:** 1353–1368, 1998

Key words: polymer foaming; cellular structure prediction; bubble nucleation; bubble growth; bubble growth in viscoelastic media

INTRODUCTION

Since their origin in the 1930s, cellular plastics or polymeric foams have received wide utility in many industrial and consumer applications. Their low material costs, high strength-to-weight ratios, wide range of properties, and ease of processing are particularly attractive. These materials can have average cell sizes ranging from a few microns to hundreds of microns. Bulk foam densities can be quite low, sometimes down to values of less than one-hundredth of the base polymer.[1] Microcellular foams, which are polymeric foams with bubble sizes in the neighborhood of 10 μm or less, are unique cellular materials in which voids smaller than the preexisting flaws in the polymers are nucleated, resulting in material cost savings without significant reductions in mechanical properties or with some improved properties.[2] The mechanical, thermal, and electrical properties of bulk foam are tied to foam density, cell structure, and base polymer properties.[1] For any given polymer, the use of different blowing agents and process conditions can produce "new materials" with different densities, structures, and properties.

With the ever mounting environmental pressures, the polymer foaming industry is in crisis because existing process technologies are based largely on the use of chlorofluorocarbons (CFCs) and volatile organic compounds (VOCs) as blowing agents.[3,4] With the ratification of the Montreal protocol, many foam producers switched from

Correspondence to: J. G. Lee.
* *Present address:* The Stone & Webster Company, Houston, TX.
† *Present address:* Shell Development Company, P.O. Box 1380, Houston, TX 77251.
‡ *Present address:* The Dow Chemical Company, Freeport, TX.
§ *Present address:* College of Engineering, University of Alabama, Tuscaloosa, AL 35487.
Contract grant sponsor: Texas Advanced Technology Program; contract grant number: 999903-274.
Journal of Applied Polymer Science, Vol. 67, 1353–1368 (1998)
© 1998 John Wiley & Sons, Inc. CCC 0021-8995/98/081353-16

CFCs to VOCs or mixtures of VOCs and inert gases. These producers are now facing increasingly strict VOC regulations by EPA and OSHA and state regulatory agencies because VOCs are suspected carcinogens, are flammable, and contribute to smog. To protect workers and to minimize emissions, expensive plant ventilation and gas collections systems are required. Producers have already been making environmentally negative adjustments by lobbying for less stringent requirements or by moving operations out of the country.

In many cases, existing process practices involve more art than science. The highly soluble CFCs and VOCs are very effective blowing agents, and their replacement by inert blowing agents (N_2, CO_2, Ar, etc.) is nontrivial. In most cases, these gases are less soluble and it is difficult to achieve the spectrum of densities and structures desired. Even with the more soluble gases (e.g., CO_2), melt rheology is affected and it is difficult to stabilize low density foam films.

A typical polymer foaming process involves several steps: the contact and dissolution under an elevated pressure $P_0^{(D)}$ of a gas blowing agent in the molten polymer; the nucleation of a dense population of gas clusters of radius R in the supersaturated solution upon the sudden release of pressure to the ambient pressure $P^{(C)}$; the growth of the nucleated bubbles in the polymer to their ultimate equilibrium size; and the quenching of the foamed material to permanently fix the structure. The dissolution of the blowing agent is generally accomplished under pressure in special melt extruders,[5] and nucleation and bubble growth occur upon depressurization at the exit die. Quenching is achieved by passing the product through a low temperature water bath. The final foam density depends on the original gas loading, the gas losses to the environment, and the foam expansion at quenching. The cell size and the cell size distribution depend on the intensity and kinetics of nucleation, the characteristics of the bubble growth processes following nucleation, and the degree of cell wall collapse, or cell coalescence, during expansion.

The work of Street et al.[6] established the initial framework for analyzing free expansion bubble growth. These investigators introduced a finite influence volume (or cell) around each bubble and analyzed the coupled mass, momentum, and energy balance equations for bubble growth in each cell. Their work focused on the initial growth stages and assumed the liquid to be a viscous power-law fluid. Since this early work, a number of extensions have been published. These have included improved cell descriptions and more realistic conditions at the outer cell boundary,[7] inclusion of viscoelastic effects,[8,9] analysis of bubble growth during process flow,[10–12] comparison of numerical foam expansion results with experiments,[9,12–14] and descriptions applicable to specific foam processes.[15,16]

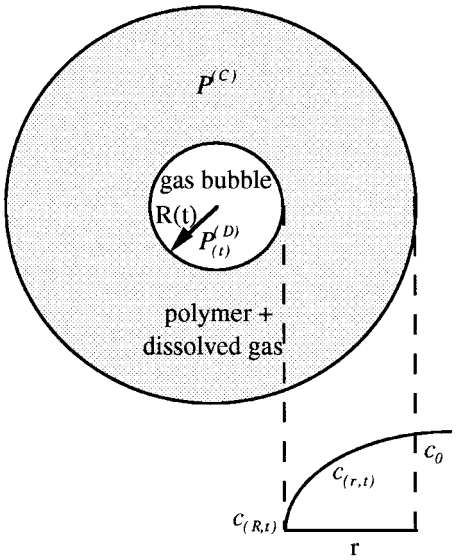

Figure 1 Schematic of single bubble growth.

Previous work on polymer foaming can be divided into studies on the two independent physical processes, namely either nucleation or bubble growth. Although many theories have been proposed for nucleation, there is no single theory that is able to predict this complex phenomenon accurately. The actual polymer foaming process is one of simultaneous nucleation and bubble growth in a highly non-Newtonian liquid. The present work incorporates simultaneous nucleation and bubble growth in a viscoelastic media through an influence volume approach. (For the application of this influence volume approach to the case of free expansion in Newtonian fluid, please see Shafi et al.[17])

MODEL DESCRIPTION AND ASSUMPTIONS

Consider a polymer melt that has a dissolved gas concentration c_0 in equilibrium with the gas at some elevated pressure $P_0^{(D)}$. With the release of pressure at $t = 0$ the solution becomes supersaturated and nucleation and bubble growth begin. As

bubble growth proceeds, the pressure inside the bubble and the dissolved gas concentration at the bubble surface decrease. With time, gas diffuses into the bubble and a concentration gradient propagates radially in the polymer melt. A schematic of the bubble growth is shown in Figure 1. The radius, pressure, and the dissolved gas concentration are denoted by $R(t)$, $P_{(t)}^{(D)}$, and $c(r, t)$.

In analyzing the growth process, we impose the following restrictions:

1. The bubble is spherically symmetric when it nucleates and remains so for the entire period of growth. (For experimental results, see Ruengphrathuengsuka.[18])
2. The gas pressure in the bubble $P_{(t)}^{(D)}$ is related to the dissolved gas concentration at the bubble surface $c(R, t)$ by

$$c(R, t) = K_H P_{(t)}^{(D)} \tag{1}$$

   Here K_H is the solubility coefficient.[19]
3. The material properties are assumed constant throughout the liquid at its initial value until foaming stops.
4. Neglect the effect of gravity and the bubble remains stationary throughout its growth period.
5. Thermal effects such as the latent heat of solution are of negligible importance during bubble growth and the growth process can be considered as isothermal.
6. Assume creeping flow and the fluid is assumed to be incompressible.
7. There is no loss of dissolved gas to the surroundings.
8. The bubbles do not mutually interact or coalesce. The bubble boundaries do not overlap during the entire process. There is no gas that remains bounded in the polymer; foaming occurs until complete chemical and mechanical equilibria are achieved.
9. The initial bubble growth state corresponds to the upper bound of the critical nucleation state under elastic deformation.[20,21]
10. The Larson viscoelastic model is used to describe the material behavior for bubble growth. It describes various deformation behaviors well, including the extensional rheology of molten polymers, and is particularly well suited to commercial, highly branched melts such as low-density polyethylene (LDPE).[22,23]

The secondary importance of the heat transport effects in the bubble growth analysis was demonstrated by Street et al.[6] It is also supported by experimental results.[24]

GOVERNING EQUATIONS FOR SINGLE BUBBLE GROWTH

Overall Mass Balance in Melt

The overall mass balance in the melt leads to

$$\nu_r = \frac{\dot{R}R^2}{r^2} \tag{2}$$

where $\dot{R}$ is the radial growth rate of the bubble and ν_r is the radial component of melt velocity.

Momentum Balance in Melt

In view of the assumptions listed earlier, the equation of differential momentum balance in the melt reduces to

$$P^{(D)} - P^{(C)} - \frac{2\gamma}{R} + 2\int_R^\infty \frac{\tau_{rr} - \tau_{\theta\theta}}{r}\, dr = 0 \tag{3}$$

Here $P^{(D)}$ is pressure in the dispersed phase, $P^{(C)}$ is pressure in the continuous phase, and γ is surface tension. The normal stresses τ_{rr} and $\tau_{\theta\theta}$ are described by the constitutive equation characterizing the liquid. For a Larson viscoelastic fluid (see Larson,[25] p. 204), these are given by a set of differential equations for each mode of the relaxation spectrum in the material coordinates, $\xi = (r^3 - R^3)/3$.

$$\frac{d\tau_{rr}^k}{dt} = -4\dot{\varepsilon}_b(G_k + \tau_{rr}^k) - \frac{\tau_{rr}^k}{\lambda_k} - \frac{4}{3}\frac{\alpha}{G_k}\dot{\varepsilon}_b(\tau_{\theta\theta}^k - \tau_{rr}^k)(G_k + \tau_{rr}^k) \tag{4}$$

$$\frac{d\tau_{\theta\theta}^k}{dt} = 2\dot{\varepsilon}_b(G_k + \tau_{\theta\theta}^k) - \frac{\tau_{\theta\theta}^k}{\lambda_k} - \frac{4}{3}\frac{\alpha}{G_k}\dot{\varepsilon}_b(\tau_{\theta\theta}^k - \tau_{rr}^k)(G_k + \tau_{\theta\theta}^k) \tag{5}$$

where the biaxial extensional rate is $\dot{\varepsilon}_b = \dot{R}R^2/r^3$, τ_{rr}^k and $\tau_{\theta\theta}^k$ are the normal stresses corresponding to the kth mode of the relaxation spectrum, G_k is the relaxation modulus of the kth mode, λ_k

is the relaxation time of the kth mode, and α is the strain softening factor in the Larson viscoelastic model. The initial conditions for the above equations are

$$R_{(0)} = R_i \quad \tau^k_{rr_{(r,0)}} = \tau^k_{rr,i_{(r)}} \quad \tau^k_{\theta\theta_{(r,0)}} = \tau^k_{\theta\theta,i_{(r)}} \quad (6)$$

Species Mass Balance in Melt and Mass Balance in Bubble

The species mass balance in the melt and mass balance in the bubble lead to

$$\frac{\partial c}{\partial t} + \frac{\dot{R}R^2}{r^2}\frac{\partial c}{\partial r} = \frac{D}{r^2}\frac{\partial}{\partial r}\left(r^2\frac{\partial c}{\partial r}\right) \quad (7)$$

$$\frac{d}{dt}\left(\frac{4\pi}{3}\frac{P^{(D)}R^3}{Z_2\Re T}\right) = 4\pi R^2 D\left.\frac{\partial c}{\partial r}\right|_{r=R} \quad (8)$$

Here c is the dissolved gas concentration in the melt, D is the binary diffusion coefficient, and Z_2 is the compressibility factor of the gas inside the bubble. The corresponding initial and boundary conditions are

$$c(r, 0) = c_i(r) \quad c(R, t) = c_R(t) = K_H P^{(D)}(t)$$
$$c(\infty, t) = c_0 \qquad P^{(D)}(0) = P_i^{(D)} \quad (9)$$

where c_R is the dissolved gas concentration at the bubble surface, K_H is the solubility coefficient, $P^{(D)}(t)$ is the pressure inside the bubble, c_0 is the dissolved gas concentration before the onset of nucleation, and $P_i^{(D)}$ is the initial bubble pressure.

INITIAL CONDITIONS FOR BUBBLE GROWTH

The maximum in the work for cluster formation acts as a barrier to nucleation. A cluster smaller than the critical cluster has a tendency to collapse and can overcome the barrier only through thermodynamic fluctuations. On the other hand, a cluster slightly larger than the critical cluster has a tendency to grow but can fall back across the barrier to a subcritical state because of thermodynamic fluctuations. If the cluster is sufficiently large compared to the critical cluster, the thermodynamic fluctuations are unable to prevent the subsequent growth and the cluster will grow spontaneously to a macroscopic bubble.

The initial conditions refer to the conditions surrounding the bubble when it has grown from its critical radius to a size such that its further growth is governed by transport effects. A cluster is considered to be nucleated when it reaches a supercritical state where the thermodynamic fluctuations cannot drive it back to subcritical conditions; then the initial radius is defined as the upper bound in the critical zone.[26] The equation for the initial conditions using the Zeldovich approach is given by[21,27]

$$P_i^{(D)}R_i^3 = P_{\mathrm{cr},0}^{(D)}R_{\mathrm{cr}}^3 \times\left[1 + \frac{3}{8\sqrt{\gamma^3/(k_{\mathrm{B}}T(P_{\mathrm{cr},0}^{(D)} - P^{(C)})^2)}}\right] \quad (10)$$

$P_{\mathrm{cr},0}^{(D)}$ refers to the original supersaturation pressure, R_{cr} is the critical radius, $P_i^{(D)}$ is the initial pressure inside the nucleated cluster, R_i is the initial radius of the nucleated cluster, k_{B} is the Boltzmann constant, and T is absolute temperature. Bubble growth is a strong function of initial conditions, and an arbitrary choice can lead to considerable error.[20]

While deriving the expression for nucleation rate, it was assumed that the cluster grows to the supercritical radius in a very short time. (The time that a cluster will take to grow from critical size to the upper bound of the critical region is on the order of microseconds[28] and is very small compared to the average relaxation time of polymer melt.) The liquid essentially sees a continuous deformation starting from the inception of a cluster to its nucleated state. The stress in a viscoelastic liquid for fast deformations is determined by the strain and not the strain path. Thus, the stress distribution in the liquid surrounding the nucleated cluster is its elastic response to rapid deformations. The pressure $P_i^{(D)}$ inside the nucleated bubble of radius R_i can be obtained by solving eq. (10) simultaneously with the relation

$$P_i^{(D)} - P^{(C)} - \frac{2\gamma}{R_i} + 2\int_{R_i}^{\infty}\frac{\tau_{rr} - \tau_{\theta\theta}}{r}\,dr = 0 \quad (11)$$

where

$$\tau_{rr} - \tau_{\theta\theta} = \frac{[(1-\vartheta^3)^{4/3} - (1-\vartheta^3)^{-2/3}]}{1 + \alpha[(1-\vartheta^3)^{4/3} + 2(1-\vartheta^3)^{-2/3} - 3]/3}\sum_{k=1}^{m} G_k$$

The variable ϑ is defined as $\vartheta = R/r$. The state of

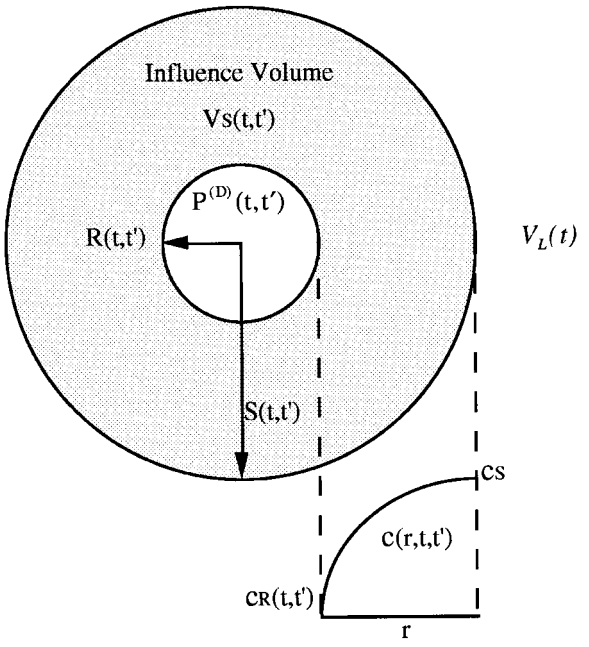

Figure 2 Schematic of a cell (bubble and its influence volume).

the cluster at the upper bound of the critical region provides the starting point for bubble growth.

SIMULTANEOUS NUCLEATION AND BUBBLE GROWTH

At any time t the radius of the bubble that nucleated at time t' is denoted by $R(t, t')$. The quantity $S(t, t')$ denotes the radial position in the melt where the dissolved gas concentration is equal to the nucleation threshold c_S. The latter is defined as the dissolved gas concentration at which the nucleation rate is 1% of the nucleation rate at the initial dissolved gas concentration. (This criteria was adopted from the boundary layer theory. For a reference, please see Geankoplis.[29]) The volume of the liquid between the bubble surface and $S(t, t')$ is called the influence volume and is denoted by $V_S(t, t')$. The bubble and its surrounding influence volume constitute a cell. A schematic of the cell is shown in Figure 2.

The volume of the melt outside (i.e., the residual volume of bubbles) is denoted by $V_L(t)$. As the dissolved gas concentration within the influence volume is below the nucleation threshold, new bubbles nucleate only in the residual region. The nucleation stops when all the liquid has been occupied by the influence regions of the growing bubbles. At this point, the cell structure has attained its final shape and the value of V_S for each bubble remains fixed. The bubbles keep on growing by consuming gas from their influence volumes until equilibrium is established between the bubbles and their surrounding influence regions. The size distribution of the cellular structure is then determined from these final bubble states.

The nucleation model used in this analysis is the extended form of nucleation theory. It included the dissolved gas, small critical cluster size, and elastic and nonideal solution effects and takes the following form:

$$J_S = N\left(\frac{2\gamma}{\pi m E}\right)^{1/2} \exp\left\{-\frac{16\pi\gamma^3}{3k_B T(P^{(D)} - P^{(C)} - I_{(G_k,\alpha)} + P^{(D)}\ln \Omega_2/Z_{2L})^2}\right\} \tag{12}$$

(For derivation and other details, please see Lee[27] and Lee and Flumerfelt.[30]) Here J_S is the steady-state homogeneous nucleation rate, N is the number of dissolved gas molecules per unit volume, γ is the surface tension at critical cluster size for the molten polymer with dissolved gas solute,[30] m is the mass of a gas molecule, E is a coefficient, k_B is the Boltzmann constant, T is the absolute temperature, $I_{(G_k,\alpha)}$ is the elasticity number of nucleation, Ω_2 is the activity coefficient of dissolved gas solute in the polymer melt, and Z_{2L} is the compressibility factor of dissolved gas solute in molten polymer. While the form of classical nucleation theory is[31–34]

$$J_{S,\text{clas}} = N\left(\frac{2\sigma_{\text{PM}}}{\pi m E}\right)^{1/2} \exp\left(-\frac{16\pi\sigma_{\text{PM}}^3}{3k_B T(P^{(D)} - P^{(C)})^2}\right) \tag{13}$$

where $J_{S,\text{clas}}$ is the steady-state homogeneous nucleation rate derived from the classical nucleation theory and σ_{PM} is the macroscopic surface tension of pure polymer melt. Then the nucleation threshold c_S derived from extended nucleation theory is given by

$$0.01 = \frac{c_S}{c_0} \exp\left[\frac{16\pi\gamma^3}{3k_B T}\left\{\frac{1}{(P_0^{(D)} - P^{(C)} - I_{(G_k,\alpha)} + P_0^{(D)}\ln \Omega_2/Z_{2L})^2} - \frac{1}{(P^{(D)} - P^{(C)} - I_{(G_k,\alpha)} + P^{(D)}\ln \Omega_2/Z_{2L})^2}\right\}\right] \tag{14}$$

Table I Base Values of Parameters for LDPE–N_2 System

Diffusion coefficient, $D = 4.26 \times 10^{-9}$ m^2 s^{-1}
Parameter in Larson model, $\alpha = 0.39$
Solubility coefficient, $K_H = 3.61 \times 10^{-5}$ mol N^{-1} m^{-1}
Surface tension at critical cluster, $\gamma = 11.5$ mN m^{-1}
Loading pressure, $P_0^{(D)} = 1.11 \times 10^7$ Pa
Ambient pressure, $P^{(C)} = 1.01 \times 10^5$ Pa
Temperature, $T = 423.8$ K
Compressibility factor of
Dissolved gas in polymer melt, $Z_{2L} = 4.46$
Gas in bubble, $Z_2 = 1.03$
Activity coefficient of dissolved gas in polymer melt, $\Omega_2 = 0.497$

Here $P_0^{(D)}$ is the initial pressure in the dispersed phase. For the base conditions listed in Table I, the nucleation threshold c_S is 96.32% of the initial dissolved gas concentration c_0. The influence volume $V_S(t, t')$ and the radius of influence volume $S(t, t')$ are given as

$$V_{s(t,t')} = \frac{4\pi}{3}(S^3_{(t,t')} - R^3_{(t,t')}) \tag{15}$$

The residual volume $V_{L(t)}$ and the total number of bubbles $N_B(t)$ at any time t are given as

$$V_L(t) = V_{L,0} - \int_0^t J_S(t')V_L(t')V_S(t, t')\,dt' \tag{16}$$

$$\frac{dN_B(t)}{dt} = J_S(t)V_L(t) \tag{17}$$

with the initial conditions

$$V_L(0) = V_{L,0} \quad N_B(0) = 0 \quad J_S(0) = J_{S,0} \tag{18}$$

where $V_{L,0}$ is the residual volume before the onset of nucleation and is equal to the melt volume and $J_{S,0}$ is the initial nucleation rate.

In the residual region there are small concentration variations with respect to space as well as time. Because the nucleation rate J_S is very sensitive to the dissolved gas concentration, we evaluate it at the average concentration c_{avg} in the residual region. c_{avg} is determined through the gas mass balance over the bubbles and the melt.

$$c_{\text{avg}}V_L = c_0V_{L,0} - \int_0^t \frac{4\pi}{3} J_S(t') \times V_L(t') \frac{P^{(D)}(t, t')R^3(t, t')}{Z_2\Re T}\,dt' - \int_0^t J_S(t')V_L(t') \times \int_{R(t,t')}^{S(t,t')} 4\pi r^2 c(r, t, t')\,dr\,dt' \tag{19}$$

In the residual region the variations in the dissolved gas concentration are less than 4% of the initial concentration. The bubble growth dynamics is not sensitive to dissolved gas concentration changes of this magnitude. We then assume that all the nucleated bubbles see the same initial and boundary conditions for growth. At any time t, the state of a bubble that nucleated at time t' can be related to that of the bubble nucleated at time zero through the following equations[17]:

$$\begin{aligned} R(t, t') &= R(t - t', 0) = R(t - t') \\ P^{(D)}(t, t') &= P^{(D)}(t - t', 0) = P^{(D)}(t - t') \\ V_{\text{cb}}(t, t') &= V_{\text{cb}}(t - t', 0) = V_{\text{cb}}(t - t') \\ V_S(t, t') &= V_S(t - t', 0) = V_S(t - t') \end{aligned} \tag{20}$$

The volume of the concentration boundary V_{cb} is defined as the melt volume between the bubble surface and the radial position in the melt where the dissolved gas concentration equals the initial dissolved gas concentration. At equilibrium ($t = t_f$) the bubbles stop growing due to a balance of pressure and surface forces, $R(t_f, t') = 2\gamma/(P^{(D)}(t_f, t') - P^{(C)})$, and the dissolved gas concentration in an influence region is uniform and is in chemical equilibrium with the pressure in the bubble it envelopes [$c_f(t_f, t') = K_HP^{(D)}(t_f, t')$]. Thus, at equilibrium the gas within the bubble and its influence volume equals the initial gas mass in the influence volume ($t = 0$).

$$c_0V_S(t_f, t') = K_HP^{(D)}(t_f, t')V_S(t_f, t') + \frac{4\pi}{3}\frac{P^{(D)}(t_f, t')R^3(t_f, t')}{Z_2\Re\text{T}} \quad \mathcal{JONJ}$$

where t_f is the time when the final cell structure was formed. The above equation is to be solved for all bubbles nucleated at different times.

DIMENSIONLESS FORMS OF NUCLEATION AND BUBBLE GROWTH EQUATIONS

The choice of dimensionless quantities arises from prior studies on bubble growth.[20,21] All quantities with an asterisk indicate dimensionless quantities.

$$c_R^* = \frac{c_R - K_H P^{(C)}}{c_0 - K_H P^{(C)}} \quad J_S^* = J_S/J_{S,0} \quad V_{\text{cb}}^* = \frac{3V_{\text{cb}}}{4\pi R_c^3}$$

$$V_L^* = V_L/V_{L,0} \quad V_S^* = \frac{3V_S}{4\pi R_c^3} \quad c^* = \frac{c - K_H P^{(C)}}{c_0 - K_H P^{(C)}}$$

$$P^{(D)*} = \frac{P^{(D)} - P^{(C)}}{P_0^{(D)} - P^{(C)}} = c_R^* \quad r^* = \frac{r}{R_c} \quad R^* = \frac{R}{R_c}$$

$$t^* = \frac{t}{t_c} \quad \xi^* = \frac{r^{*3} - R^{*3}}{3} \quad \dot{\varepsilon}_b^* = \frac{\dot{\varepsilon}_b}{1/t_c}$$

$$c_S^* = \frac{c_S - K_H P^{(C)}}{c_0 - K_H P^{(C)}} \quad N_{\text{G}} = \frac{16\pi\gamma^3}{3k_{\text{B}}T(P_0^{(D)} - P^{(C)})^2}$$

$$N_{\text{Pe}} = \frac{\gamma^2}{\eta D(P_0^{(D)} - P^{(C)})} \quad N_{\text{PI}} = \frac{P^{(C)}}{P_0^{(D)} - P^{(C)}}$$

$$N_{\text{SI}} = K_H \Re T \quad \tau_{rr}^{k*} = \frac{\tau_{rr}^k}{P_0^{(D)} - P^{(C)}}$$

$$\tau_{\theta\theta}^{k*} = \frac{\tau_{\theta\theta}^k}{P_0^{(D)} - P^{(C)}} \quad (22)$$

Here viscosity $\eta = \sum_{i=1}^{m} \lambda_i G_i$. In defining the above dimensionless quantities, we picked the critical bubble radius from classical nucleation theory, $R_c = 2\gamma/(P_0^{(D)} - P^{(C)})$, and the critical momentum transfer time, $t_\eta = 4\eta/(P_0^{(D)} - P^{(C)}) = t_c$, as our characteristic bubble radius and bubble growth time. $\bar{\lambda}$ is the average relaxation time defined as[35]

$$\bar{\lambda} = \sum_{k=1}^{m} \lambda_k^2 G_k \Big/ \left(\sum_{k=1}^{m} \lambda_k G_k \right)$$

The base case values of different physical and process parameters are listed in Table I. All these parameter values either come from literature data or from our laboratory data (e.g., Ω_2,[19]) or typical operating conditions. The corresponding values of the characteristic quantities and dimensionless groups are given in Table II. The G_k and λ_k values given in Table III are obtained from the relaxation spectrum for a low density polyethylene (LDPE) melt.[25,36]

The relaxation times are dimensionless with respect to the average relaxation time $\bar{\lambda}$ (i.e., $\lambda_k^* = \lambda_k/\bar{\lambda}$). Also, the Deborah number N_{De} is defined as $N_{\text{De}} = \bar{\lambda}/t_c$. We define an average relaxation modulus $\bar{G}$ to convert the G_ks to dimensionless units (i.e., $\bar{G} = \eta/\bar{\lambda}$ and $G_k^* = G_k/\bar{G}$).

In terms of dimensionless quantities, the governing equations take the following forms.

Single Bubble Growth Dynamics

$$c_R^* - \frac{1}{R^*} + 2\int_0^\infty \frac{\tau_{rr}^* - \tau_{\theta\theta}^*}{(3\xi^* + R^{*3})}\, d\xi^* = 0 \quad (23)$$

$$\frac{\partial c^*}{\partial t^*} + \frac{R^{*2}}{r^{*2}} \frac{dR^*}{dt^*} \frac{\partial c^*}{\partial r^*} = \frac{1}{N_{\text{Pe}} r^{*2}} \frac{\partial}{\partial r^*} \left(r^{*2} \frac{\partial c^*}{\partial r^*} \right) \quad (24)$$

Table II Characteristic Quantities and Base Values of Dimensionless Groups

$t_c = 1.78 \times 10^{-2}$ s
$R_c = 2.10 \times 10^{-9}$ m
$N_{De}^0 = 2.12 \times 10^3$
$N_G^0 = 3.62 \times 10$
$N_{Pe}^0 = 5.78 \times 10^{-8}$
$N_{PI}^0 = 9.18 \times 10^{-3}$
$N_{SI}^0 = 1.27 \times 10^{-1}$

Table III Relaxation Spectrum of Low Density Polyethylene

Relaxation Time λ_k (s)	Relaxation Modulus G_k (dyne/cm^2)
0.001	1.52×10^6
0.005	4.005×10^5
0.028	3.326×10^5
0.14	1.659×10^5
0.7	8.69×10^4
3.8	3.151×10^4
20	8.596×10^3
100	1.283×10^3
500	1.849×10^1

Adapted from Laun[36] and Larson.[25]

$$\frac{dc_R^*}{dt^*} = \frac{3N_{SI}Z_2}{N_{Pe}}\frac{1}{R^*}\frac{\partial c^*}{\partial r^*}\bigg|_{r^*=R^*} - \frac{3(c_R^* + N_{PI})}{R^*}\frac{dR^*}{dt^*} \quad (25)$$

The stresses are given by a pair of ordinary differential equations (ODEs) for each mode of the relaxation spectrum

$$\frac{d\tau_{rr}^{k^*}}{dt^*} = -4\dot{\varepsilon}_b^*\left(\frac{G_k^*}{4N_{De}} + \tau_{rr}^{k^*}\right) - \frac{\tau_{rr}^{k^*}}{N_{De}\lambda_k^*} - \frac{16}{3}\frac{\alpha N_{De}}{G_k^*}\dot{\varepsilon}_b^*(\tau_{\theta\theta}^{k^*} - \tau_{rr}^{k^*})\left(\frac{G_k^*}{4N_{De}} + \tau_{rr}^{k^*}\right) \quad (26)$$

$$\frac{d\tau_{\theta\theta}^{k^*}}{dt^*} = 2\dot{\varepsilon}_b^*\left(\frac{G_k^*}{4N_{De}} + \tau_{\theta\theta}^{k^*}\right) - \frac{\tau_{\theta\theta}^{k^*}}{N_{De}\lambda_k^*} - \frac{16}{3}\frac{\alpha N_{De}}{G_k^*}\dot{\varepsilon}_b^*(\tau_{\theta\theta}^{k^*} - \tau_{rr}^{k^*})\left(\frac{G_k^*}{4N_{De}} + \tau_{\theta\theta}^{k^*}\right) \quad (27)$$

Here

$$\dot{\varepsilon}_b^* = \frac{R^{*2}}{3\xi^* + R^{*3}}\frac{dR^*}{dt^*}$$

with the initial conditions as

$$R^*(t=0) = R_i^* \quad c_R^*(t=0) = c_{R,i}^* \quad (28)$$

$$\tau_{rr}^*(t=0) = \tau_{rr,i}^* = \frac{(\upsilon^{4/3} - 1)}{1 + \alpha(\upsilon^{4/3} + 2\upsilon^{-2/3} - 3)/3}\frac{1}{4N_{De}}\sum_{k=1}^{m} G_k^* \quad (29)$$

$$\tau_{\theta\theta}^*(t=0) = \tau_{\theta\theta,i}^* = \frac{(\upsilon^{-2/3} - 1)}{1 + \alpha(\upsilon^{4/3} + 2\upsilon^{-2/3} - 3)/3}\frac{1}{4N_{De}}\sum_{k=1}^{m} G_k^* \quad (30)$$

where

$$\upsilon = \frac{3\xi^*}{3\xi^* + R^{*3}}$$

The subscript i refers to the initial value of the variable. The equations specifying the initial radius R_i^* and the dimensionless concentration $c_{R,i}^*$ around a nucleated bubble take the following dimensionless forms:

$$(N_{PI} + c_{R,i}^*)R_i^{*3} = (1 + N_{PI})\left(1 + \frac{\sqrt{3\pi}}{2\sqrt{N_G}}\right) \quad (31)$$

$$c_{R,i}^* - \frac{1}{R_i^*} + 2\int_0^\infty \frac{\tau_{rr,i}^* - \tau_{\theta\theta,i}^*}{3\xi^* + R_i^{*3}}\,d\xi^* = 0 \quad (32)$$

where the stress is defined as the elastic response to deformation

$$\tau_{rr,i}^* - \tau_{\theta\theta,i}^* = \frac{(\upsilon^{4/3} - \upsilon^{-2/3})}{1 + \alpha(\upsilon^{4/3} + 2\upsilon^{-2/3} - 3)/3}\frac{1}{4N_{De}}\sum_{k=1}^{m} G_k^*$$

Nucleation Threshold

$$0.01 = \frac{c_s^* + N_{PI}}{1 + N_{PI}} \times \exp\left[N_G\left\{\frac{1}{(1 - I_{(G_k^*,\alpha)} + (1 + N_{PI})\ln\,\Omega_2/Z_{2L})^2} - \frac{1}{(c_s^* - I_{(G_k^*,\alpha)} + (c_s^* + N_{PI})\ln\,\Omega_2/Z_{2L})^2}\right\}\right] \quad (33)$$

where

$$I_{(G_k^*,\alpha)} = \int_0^1 \frac{9}{2\alpha}\ln[1 + \alpha((1 - \vartheta^3)^{4/3} + 2(1 - \vartheta^3)^{-2/3} - 3)/3]\frac{d\vartheta}{\vartheta^4}\sum_{k=1}^{m}\frac{G_k^*}{4N_{De}}$$

Nucleation Rate

$$J_s^* = \frac{c_{avg}^* + N_{PI}}{1 + N_{PI}} \times \exp\left[N_G\left\{\frac{1}{(1 - I_{(G_k^*,\alpha)} + (1 + N_{PI})\ln\,\Omega_2/Z_{2L})^2} - \frac{1}{(c_{avg}^* - I_{(G_k^*,\alpha)} + (c_{avg}^* + N_{PI})\ln\,\Omega_2/Z_{2L})^2}\right\}\right] \quad (34)$$

Simultaneous Nucleation and Growth of Bubbles

$$\frac{1 - c_s^*}{1 - c_R^*} = y_S + y_S(1 - y_S) \sum_{i=0}^{M} a_i(t^*) P_i(y_s) \quad (35)$$

$$V_S^* = R^{*3}\left\{\frac{1}{y_S^3} - 1\right\} \quad (36)$$

$$V_L^*(t^*) = 1 - \beta \times \int_0^{t^*} J_S^*(t^{*\prime}) V_L^*(t^{*\prime}) V_S^*(t^* - t^{*\prime})\, dt^{*\prime} \quad (37)$$

$$\frac{dN_B}{dt^*} = \alpha\beta J_S^*(t^*) V_L^*(t^*) \quad (38)$$

$$(N_{\mathrm{PI}} + c_{\mathrm{avg}}^*) V_L^*(t^*) = (1 + N_{\mathrm{PI}}) - \frac{\beta}{Z_2 N_{\mathrm{SI}}} \int_0^{t^*} J_S^*(t^{*\prime}) V_L^*(t^{*\prime}) \{c_R^*(t^* - t^{*\prime}) + N_{\mathrm{PI}}\} R^{*3}(t^* - t^{*\prime})\, dt^{*\prime} - 3\beta \int_0^{t^*} J_S^*(t^{*\prime}) V_L^*(t^{*\prime}) R^{*3}(t^* - t^{*\prime}) \times \int_1^{y_S(t^* - t^{*\prime})} \frac{(1 + N_{\mathrm{PI}}) - C(y, t^* - t^{*\prime}) \{1 - c_R^*(t^* - t^{*\prime})\}}{y^4}\, dy\, dt^{*\prime} \quad (39)$$

with the initial conditions

$$V_L^*(0) = 1 \quad J_S^*(0) = 1 \quad N_B(0) = 0 \quad (40)$$

where $\alpha = 3V_{L,0}/4\pi R_c^3$ and $\beta = 4\pi/3\ J_{S,0} t_c R_c^3$. The derivation of eqs. (35), (36), and (39) used the Galerkin method, which will be explained in detail in the next section.

Final Bubble Size

$$N_{\mathrm{SI}} V_S^*(t_f^* - t^{*\prime})\{R_f^*(t_f^* - t^{*\prime}) + 1\} - R_f^{*3}(t_f^* - t^{*\prime})\{N_{\mathrm{PI}} R_f^*(t_f^* - t^{*\prime}) - 1\} = 0 \quad (41)$$

SOLUTION METHODOLOGY

Equations (23)–(25) can be solved independently of the equations describing the simultaneous nucleation and bubble growth. This set of simultaneous nonlinear algebraic and differential equations describe the bubble growth process. These equations are highly nonlinear and coupled and an analytical solution is not possible. Hence, a combination of numerical techniques was used to solve them.

A Galerkin method was used to convert eq. (24) to a set of ODEs in terms of the time-dependent coefficient a_i in the solution's orthogonal expansion. The dissolved gas concentration in the melt is given by

$$C = y + y(1 - y) \sum_{i=0}^{n} a_i P_i(y)$$

where P_i is the ith shifted Jacobi polynomial defined on the interval [0, 1] with respect to the weighting function $y(1 - y)$, $C = (1 - c^*)/(1 - c_R^*)$, and $y = R/r$ where $R \le r \le \infty$. The integration over the stresses in eq. (23) poses serious problems because the stress equations, eqs. (26) and (27), need to be solved over space and time for each mode of the relaxation spectrum. A Gauss–Laguerre quadrature technique[37] was used to numerically evaluate the integral over space. The stress equations were solved using the Gear's stiff method.

Further, the ODEs were converted to a set of nonlinear equations using the two-point implicit method.[38] These equations were then solved simultaneously with eq. (23) using the Broyden's method.[37,39]

The influence volumes and bubble number computations were performed using a finite difference scheme. After nucleation ends ($V_L = 0$), Broyden's method[37,39] provides a solution to eq. (41) for each cell to predict the final foam structure. Figure 3 shows the flowchart for solving the system of equations governing nucleation and bubble growth. The details of the solution process are provided elsewhere.[27]

RESULTS AND DISCUSSION

The bubble growth and nucleation processes are dependent on various materials properties and operating conditions that were expressed in an appropriate dimensionless form (N_{Pe}, N_{De}, N_{SI}, N_{PI}, N_{G}). We present sensitivity results that isolate the effect of these groups on bubble growth and foam structure. The base conditions for the simulation studies were selected for an LDPE sample foamed with nitrogen (N_2). The base data are given in Tables I–III.

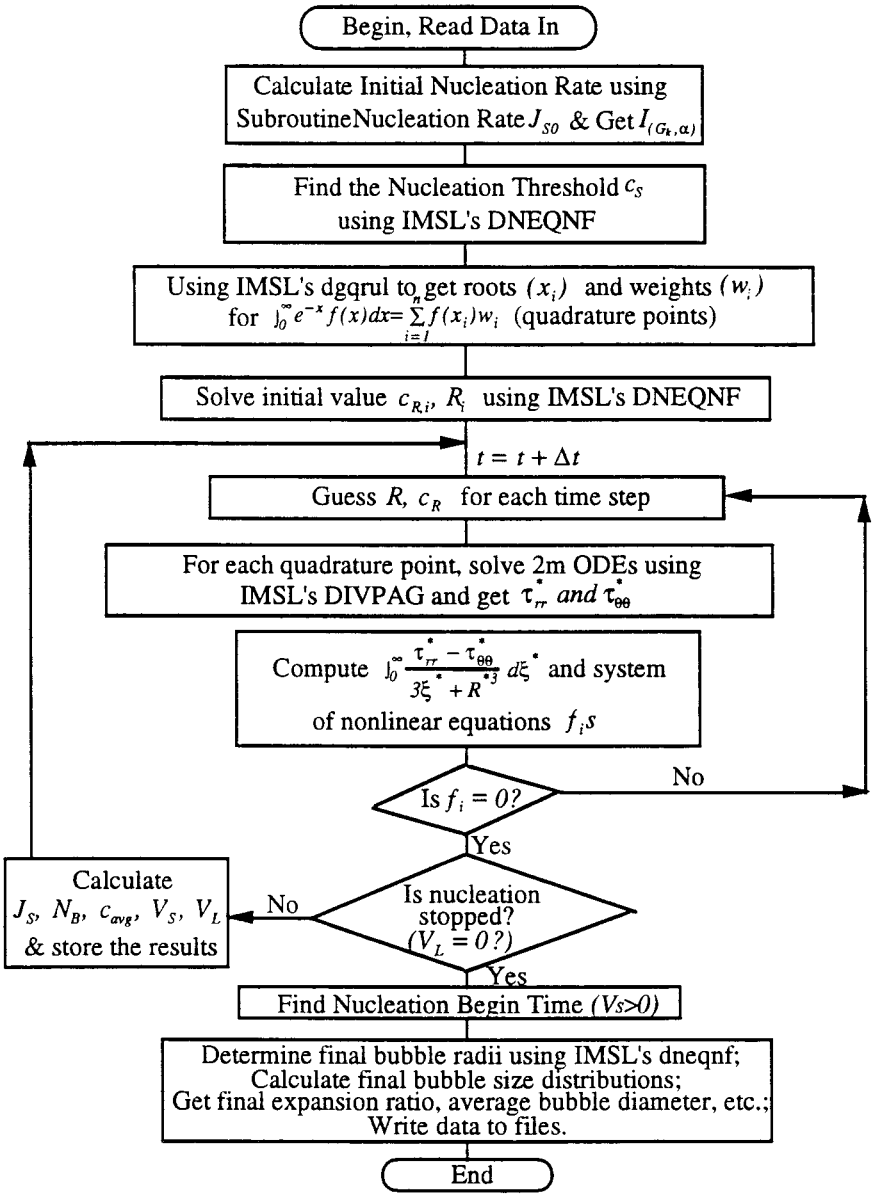

Figure 3 Flowchart for solving the system of equations governing nucleation and bubble growth in free expansion of viscoelastic media.

Single Bubble Growth in Finite Fluid

Bubble growth is a function of the dimensionless parameters N_{Pe}, N_{De}, N_{SI}, N_{PI}, and N_{G}. N_{G} is only embedded in the relationship of $c^*_{R,i}$ and R^*_i [eqs. (31) and (32)], and its effect on bubble growth is very minor. The Peclet number N_{Pe} is the ratio of the convective to the diffusive mass transfer. Decreasing the Peclet number, or increasing the diffusivity as shown in Figure 4, results in a faster delivery of gas to the surface and faster bubble growth. The bubble radius is strongly influenced by changes in the Peclet number that signify the dominance of diffusive effects.

The effect of increasing the solubility number N_{SI} is similar to decreasing the Peclet number, the former governing the availability of gas in the liquid and the latter controlling the supply of gas to the bubble surface. As shown in Figure 5, bubble growth is enhanced with a higher solubility number.

The number N_{PI} represents the ratio of the system back pressure $P^{(C)}$ to the pressure difference across the bubble surface. The initial bubble pressure difference is nearly 2 orders higher than $P^{(C)}$ and thus variation in N_{PI} does not produce different growth rates until the later times when bubble pressure is comparable to $P^{(C)}$. A lower N_{PI}

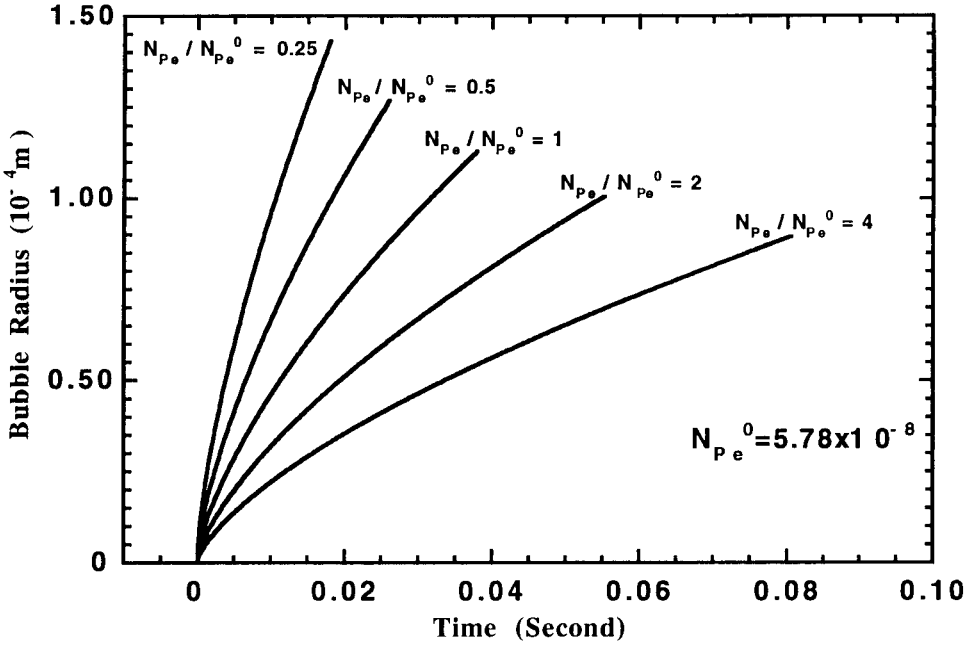

Figure 4 Effect of Peclet number on bubble growth in finite fluid.

implies a higher driving force in the later times. In Figure 6 faster growth rates are associated with lower dimensionless ambient pressure N_{PI}.

The Deborah number N_{De} was defined as the ratio of the average relaxation time $\bar{\lambda}$ of the polymer melt to the characteristic time of the growth process t_c. A high Deborah number implies the dominance of elastic forces, and a relatively low number implies the dominance of viscous forces. The bubble growth is enhanced by higher Deborah numbers in viscoelastic media (Fig. 7). The stresses developed in viscoelastic fluids are less when the Deborah number N_{De} increases and the initial growth is faster. Also observe that the ac-

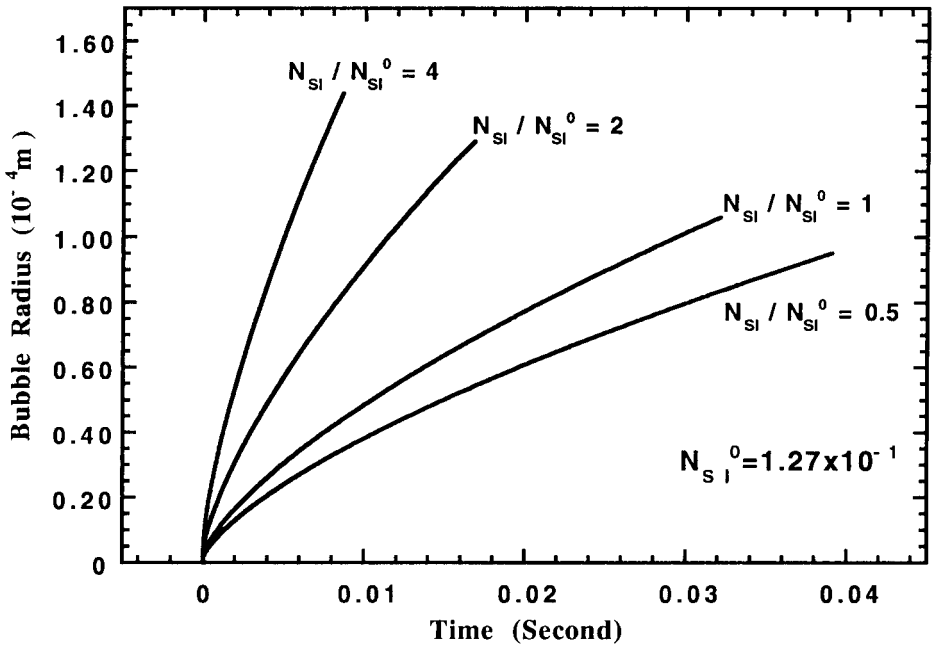

Figure 5 Effect of solubility number on bubble growth in finite fluid.

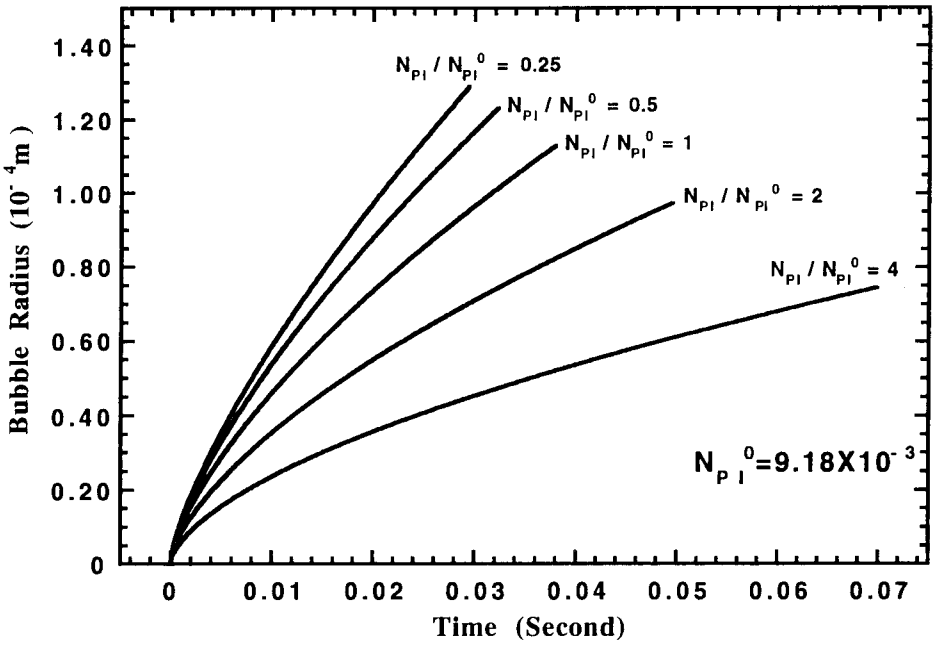

Figure 6 Effect of dimensionless ambient pressure on bubble growth in finite fluid.

celerated growth rate confirms our assumption of an elastic liquid behavior in the vicinity of nucleated bubbles. The result that melt elasticity appears to enhance bubble growth is in agreement with the observations made by other investigators on bubble growth.[40,41] When the Deborah number is sufficiently high, the rate of bubble growth in viscoelastic media is independent of the Deborah number during a free expansion process (Fig. 7).

Ultimate Foam Structure

The bubble sizes and their distribution are the quantities that characterize the foam. The bubble sizes and their distribution in the foam are dependent on the relative rates of inception and growth of the bubbles. Increasing a parameter that enhances growth results in larger bubbles with a wide distribution of sizes. A faster rate of gas con-

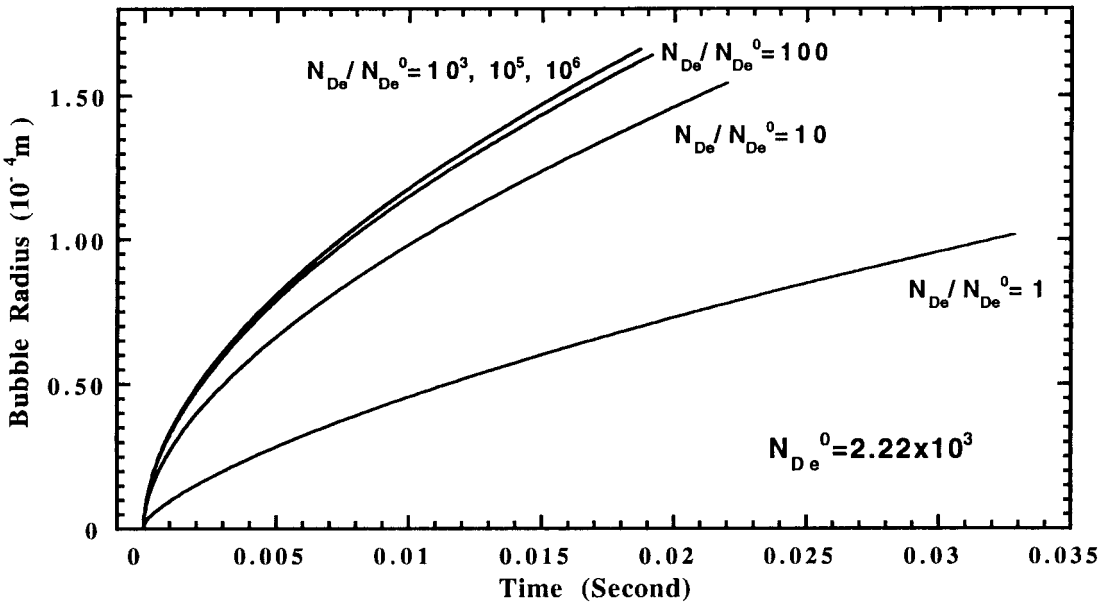

Figure 7 Effect of Deborah number on bubble growth in finite fluid.

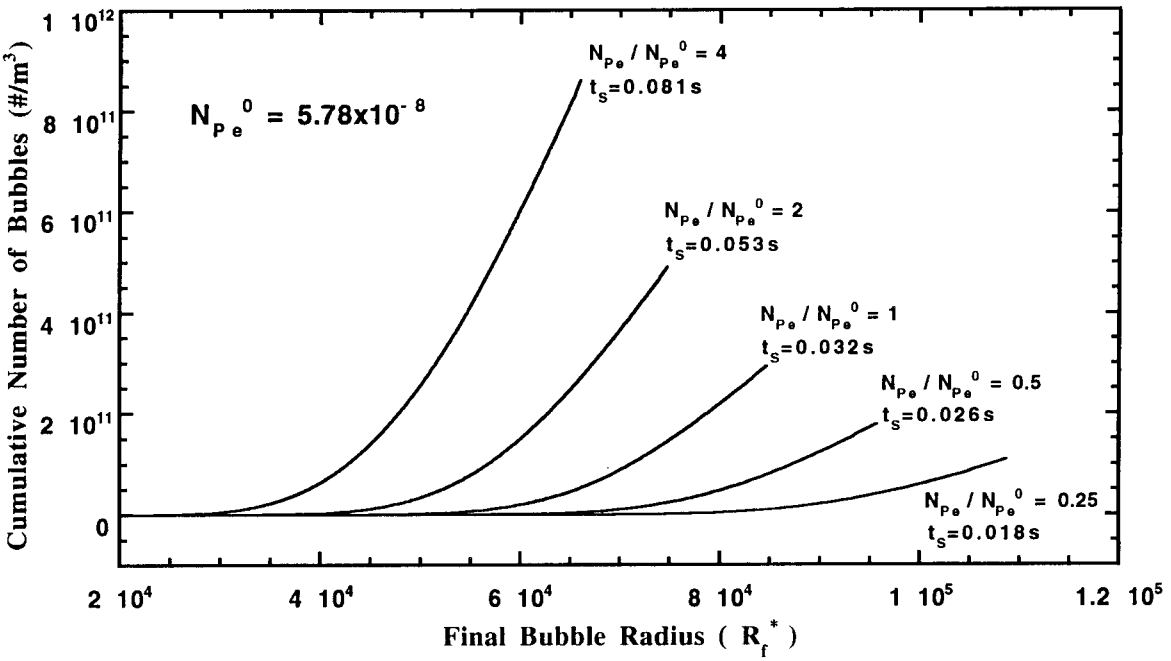

Figure 8 Effect of Peclet number on ultimate foam structure.

sumption by the growing bubbles leaves a reduced supply for nucleation. A narrower distribution and higher bubble density is expected when nucleation rates are increased. All dimensionless numbers affecting growth and/or nucleation influence the foam structure.

Lowering the Peclet number N_{Pe} enhances growth but also influences nucleation rate. The bubbles consume gas at a faster rate and the threshold concentration c_S in the entire liquid is reached earlier. The duration of nucleation t_S (i.e., the time duration until the volume of the

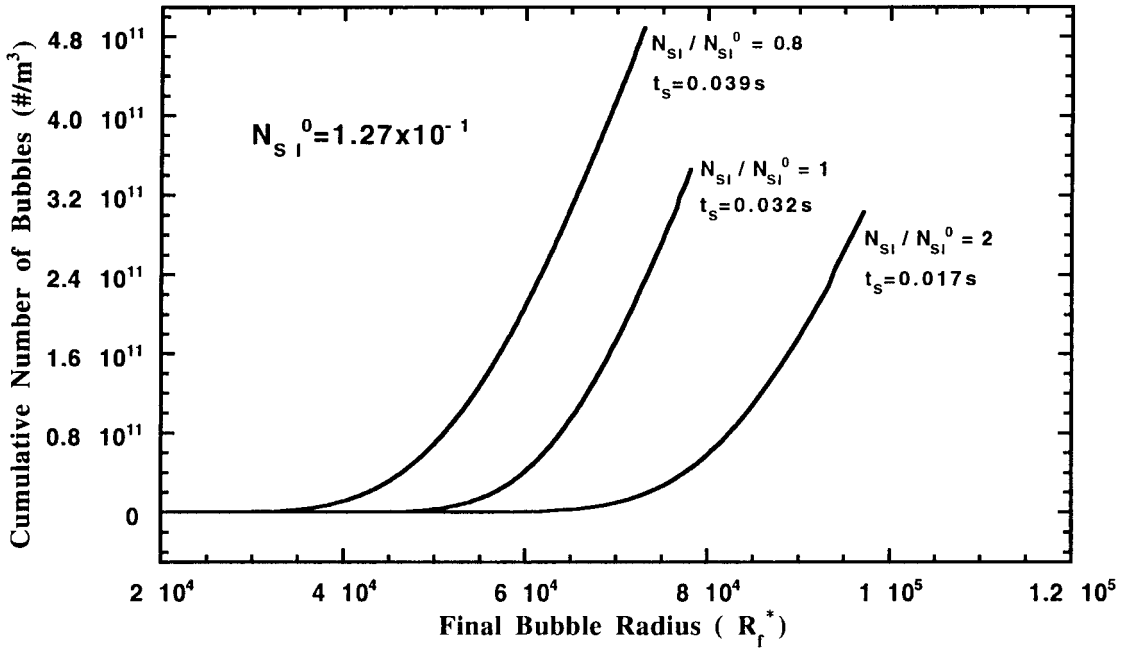

Figure 9 Effect of solubility number on ultimate foam structure.

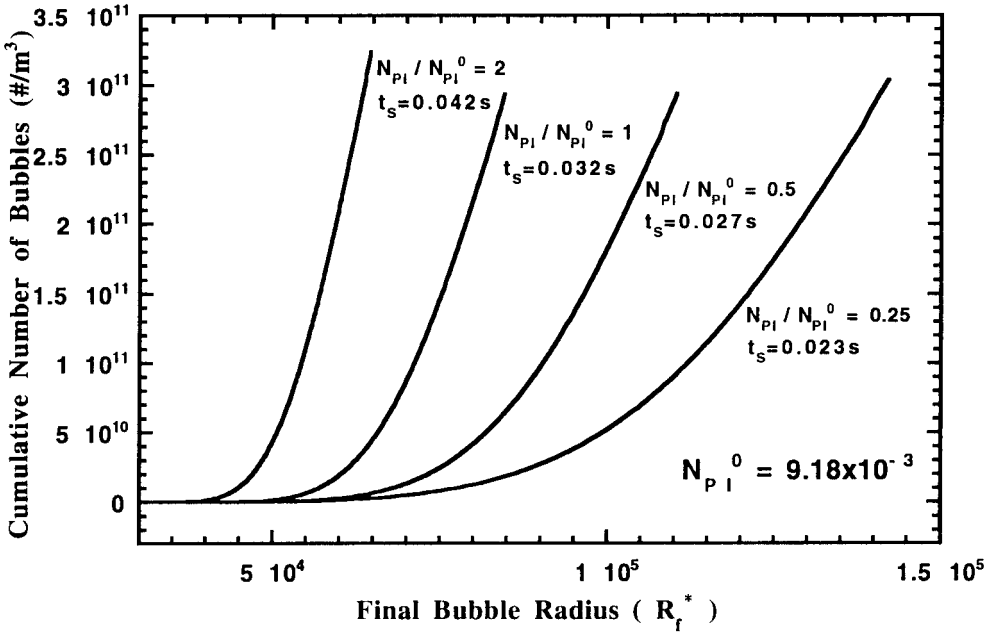

Figure 10 Effect of dimensionless ambient pressure on ultimate foam structure.

residual region equals zero) shortens as shown in Figure 8 and the cumulative number of bubbles decreases.

A high gas solubility enhances both nucleation and growth processes. The rapidly expanding boundaries compete with a higher rate of bubble nucleation. The number N_{SI} appears to influence bubble growth more because the bubble population in Figure 9 shows a slight reduction upon increasing solubility. The duration of nucleation t_S shortens with a higher N_{SI}, but there is more gas in the influence volumes when nucleation

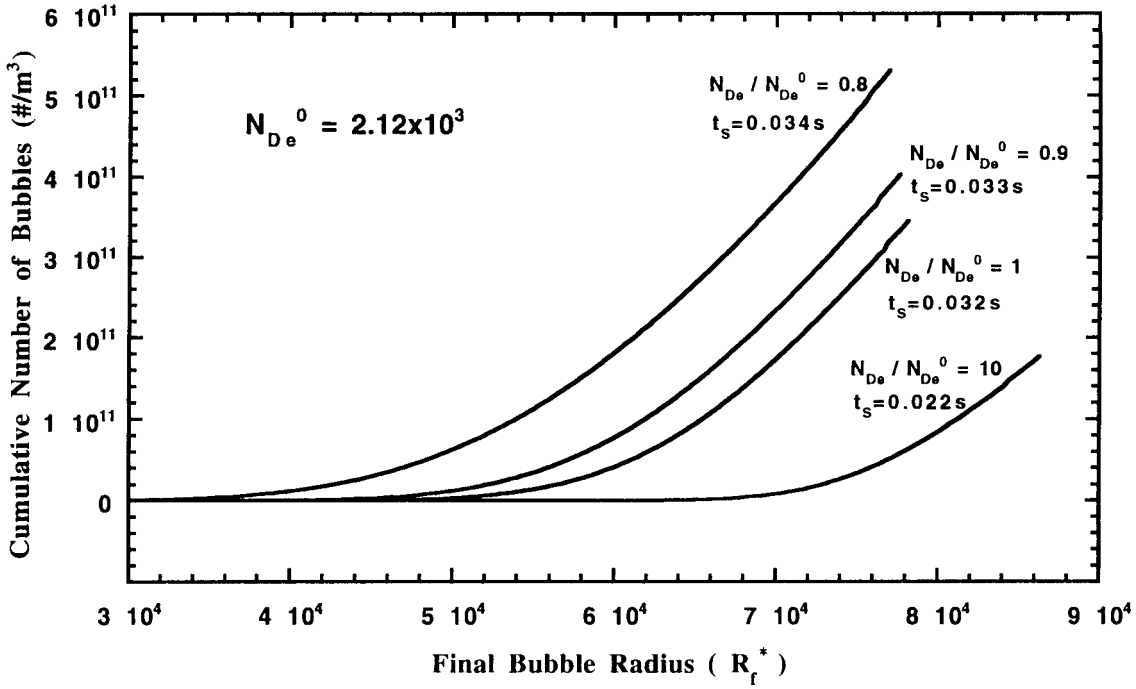

Figure 11 Effect of Deborah number on ultimate foam structure.

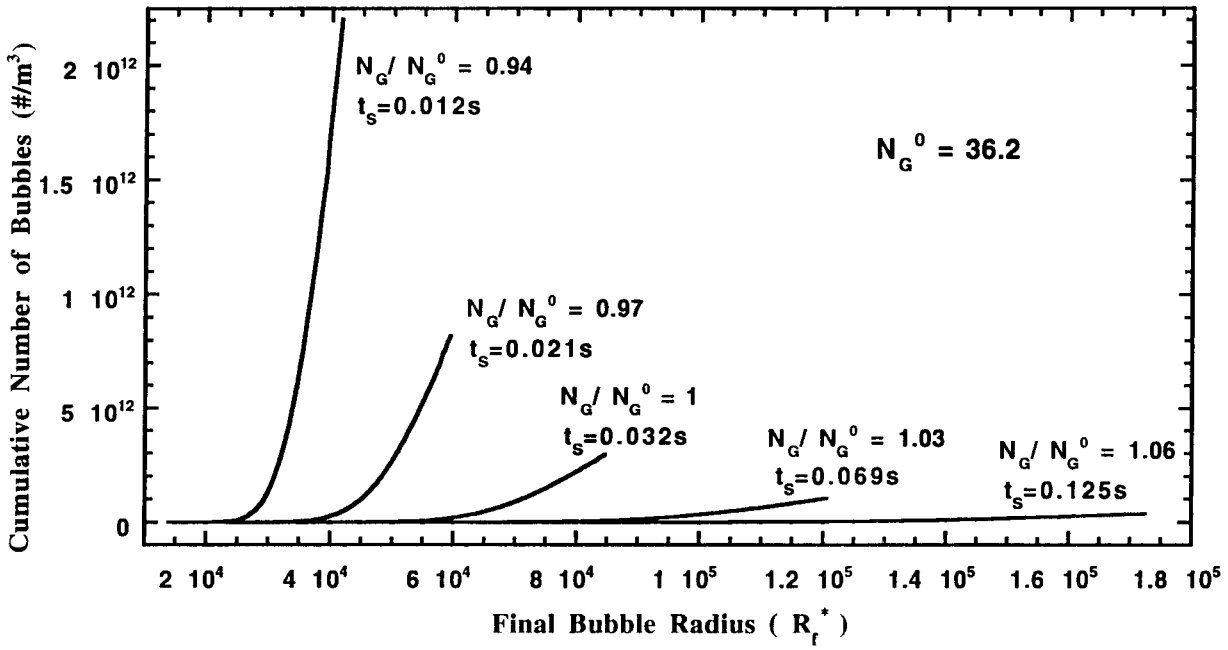

Figure 12 Effect of Gibbs number on ultimate foam structure.

ends. The result is a wide range of bubble sizes and a lower bubble density.

The dimensionless ambient pressure N_{PI} along with N_{SI} determines the amount of gas left in the liquid at equilibrium [eq. (41)]. Growth rate is inversely related to N_{PI}. As shown in Figure 10, lowering N_{PI} results in a broader bubble size distribution and a predominance of larger bubbles. At low back pressures a larger amount of gas is released, producing bigger bubbles in the foam.

Viscoelasticity hinders bubble nucleation, although to a minor extent at our base conditions. Growth rate on the other hand is accelerated under high Deborah numbers. The fast growing bubbles occupy the liquid region faster, the nucleation time decreases, and fewer bubbles nucleate. Also, in viscoelastic liquids the smaller bubbles grow at faster rates which skews the distribution in Figure 11 toward large size bubbles. At low Deborah numbers growth is relatively slow, the simultaneous growth and nucleation occur for a longer period, and a large bubble population results.

The strongest impact on the foam quality is due to the Gibbs number N_G which is a dimensionless measure of the barrier to overcome for nucleation. Nucleation is very sensitive to the variation in this number. As shown in Figure 12, a lower N_G leads to a massive increase in the number of nucleated bubbles and the liquid expanse is quickly filled with these bubbles. The time for nucleation t_S decreases, the growth of the bubbles is limited, and smaller bubbles with a high bubble number density results.

CONCLUSIONS

A systematic model of cellular structure prediction in viscoelastic media, which incorporates the simultaneous occurrence of nucleation and bubble growth, has been developed. The initial conditions correspond to the upper bound of the critical nucleation state. An influence volume approach, based on nucleation rate, is used to account for the limited supply of dissolved gas. Numerical analysis showed that bubble growth rate increases with an increase of dissolved gas diffusion in a polymer, gas solubility in a polymer, pressure difference across a bubble surface, and the relative importance of elastic to viscous effects. Factors that enhance bubble growth yield a wider range of bubble size distributions and the domination of larger bubbles. Lowering surface tension increases nucleation rate dramatically and results in a much narrower bubble size distribution and a much higher bubble density and smaller bubble sizes.

Financial support of this work was provided by the State of Texas Advanced Technology Program (Project 999903-274).

REFERENCES

1. F. A. Shutov, in *Handbook of Polymeric Foams and Foam Technology,* D. Klempner and K. C. Frisch, Eds., Hanser Publishers, New York, 1991, p. 17.
2. D. F. Baldwin, M. Shimo, and N. P. Suh, *J. Eng. Mater. Technol.,* **117,** 62 (1995).
3. S. Barlas, *Plast. World,* **44,** 21 (1986).
4. P. S. Zurer, *Chem. Eng. News,* 17 (1988).
5. E. F. Kiczek and A. I. Dalton, Jr., U.S. Pat. 5,034,171 (1991) (to Air Products and Chemicals, Inc.).
6. J. R. Street, A. L. Fricke, and L. P. Reiss, *Ind. Eng. Chem. Fundam.,* **10,** 54 (1971).
7. M. Amon and C. D. Denson, *Polym. Eng. Sci.,* **24,** 1026 (1984).
8. A. Arefmanesh and S. G. Advani, in *Processing of Polymers and Polymeric Composites,* Vol. 19, A. A. Tseng and S. K. Suh, Eds., The American Society of Mechanical Engineers, New York, 1990, p. 185.
9. N. S. Ramesh, D. H. Rasmussen, and G. A. Campbell, *Polym. Eng. Sci.,* **31,** 1657 (1991).
10. M. Amon and C. D. Denson, *Polym. Eng. Sci.,* **26,** 255 (1986).
11. A. Arefmanesh, S. G. Advani, and E. E. Michaelides, *Polym. Eng. Sci.,* **30,** 1330 (1990).
12. A. Arefmanesh and S. G. Advani, in *Cellular Polymers,* Vol. 38, V. Kumar and S. G. Advani, Eds., The American Society of Mechanical Engineers, New York, 1992, p. 25.
13. N. S. Ramesh, D. H. Rasmussen, and G. A. Campbell, *Polym. Eng. Sci.,* **34,** 1685 (1994).
14. N. S. Ramesh, D. H. Rasmussen, and G. A. Campbell, *Polym. Eng. Sci.,* **34,** 1698 (1994).
15. J. R. Youn and N. P. Suh, *Polym. Compos.,* **6,** 175 (1985).
16. S. F. Wang and A. A. Ogale, *Polym.-Plast. Technol. Eng.,* **29,** 355 (1990).
17. M. A. Shafi, J. G. Lee, and R. W. Flumerfelt, *Polym. Eng. Sci.,* **36,** 1950 (1996).
18. W. Ruengphrathuengsuka, Ph.D. Dissertation, Chem. Eng. Dept., Texas A&M University, College Station, Texas (1992), p. 121.
19. J. G. Lee and R. W. Flumerfelt, *J. Appl. Polym. Sci.,* **58,** 2213 (1995).
20. M. A. Shafi, Ph.D. dissertation, Texas A&M University, College Station, TX, 1992.
21. K. Joshi, M.S. thesis, Texas A&M University, College Station, TX, 1992.
22. R. G. Larson, *J. Rheol.,* **28,** 545 (1984).
23. S. A. Khan and R. G. Larson, *J. Rheol.,* **31,** 207 (1987).
24. S. K. Goel and E. J. Beckman, *AIChE J.,* **41,** 357 (1995).
25. R. G. Larson, *Constitutive Equations for Polymer Melts and Solutions,* Butterworths, Boston, 1988.
26. J. B. Zeldovich, *Acta Physicochem. USSR,* **18,** 1 (1943).
27. J. G. Lee, Ph.D. dissertation, Texas A&M University, College Station, TX, 1995.
28. J. Feder, K. C. Russel, J. Lothe, and G. M. Pound, *Adv. Phys.,* **15,** 111 (1966).
29. C. J. Geankoplis, *Transport Processes and Unit Operations,* 3rd ed., Prentice–Hall, Englewood Cliffs, NJ, 1993, p. 192.
30. J. G. Lee and R. W. Flumerfelt, *J. Colloid Interface Sci.,* **184,** 335 (1996).
31. M. Blander and J. L. Katz, *AIChE J.,* **21,** 833 (1975).
32. J. W. Gibbs, *The Collected Works of J. Willard Gibbs, Vol. I, Thermodynamics,* Yale University Press, New Haven, CT, 1948.
33. F. Buff, *J. Chem. Phys.,* **19,** 1591 (1951).
34. S. Kondo, *J. Chem. Phys.,* **25,** 662 (1956).
35. A. C. Papanastasiou, L. E. Scriven, and C. W. Macosko, *J. Non-Newtonian Fluid Mech.,* **16,** 53 (1984).
36. H. M. Laun, *J. Rheol.,* **30,** 459 (1986).
37. W. H. Press, S. A. Teukolsky, W. T. Vetterling, and B. P. Flannery, *Numerical Recipes in FORTRAN, The Art of Scientific Computing,* 2nd ed., Cambridge University Press, New York, 1992.
38. C. D. Holland and A. L. Liapis, *Computer Methods for Solving Dynamic Separation Problems,* McGraw–Hill, New York, 1983.
39. IMSL, *IMSL User's Manual, Fortran Subroutines for Mathematical Applications,* Houston, TX, 1991.
40. C. D. Han and H. J. Yoo, *Polym. Eng. Sci.,* **21,** 518 (1981).
41. A. Arefmanesh, Ph.D. dissertation, Univ. of Delaware, Newark, DE, 1991.